

Photochemical & Photobiological Sciences

Accepted Manuscript



This is an *Accepted Manuscript*, which has been through the Royal Society of Chemistry peer review process and has been accepted for publication.

Accepted Manuscripts are published online shortly after acceptance, before technical editing, formatting and proof reading. Using this free service, authors can make their results available to the community, in citable form, before we publish the edited article. We will replace this *Accepted Manuscript* with the edited and formatted *Advance Article* as soon as it is available.

You can find more information about *Accepted Manuscripts* in the [Information for Authors](#).

Please note that technical editing may introduce minor changes to the text and/or graphics, which may alter content. The journal's standard [Terms & Conditions](#) and the [Ethical guidelines](#) still apply. In no event shall the Royal Society of Chemistry be held responsible for any errors or omissions in this *Accepted Manuscript* or any consequences arising from the use of any information it contains.

Real-time luminescence microspectroscopy monitoring of singlet oxygen in individual cells.

Marek Scholz,^{*a} Roman Dědic,^a Jan Valenta,^a Thomas Breitenbach,^b and Jan Hála^a

A new setup for direct microspectroscopic monitoring of singlet oxygen ($^1\text{O}_2$) has been developed in our laboratory using a novel near-infrared sensitive InGaAs 2D-array detector. An imaging spectrograph has been inserted in front of the 2D-array detector, which allows us to acquire spectral images where one dimension is spatial and the other is spectral. The work presents a detailed examination of sensitivity and noise characteristics of the setup and its ability to detect $^1\text{O}_2$. The $^1\text{O}_2$ phosphorescence-based images and near-infrared luminescence spectral images recorded from single TMPyP-containing fibroblast cells reflecting spectral changes during irradiation are demonstrated. The introduction of spectral images addresses the issue of a potential spectral overlap of $^1\text{O}_2$ phosphorescence with near-infrared-extended luminescence of the photosensitizer and provides a powerful tool for their distinguishing and separation, which can be applied to any photosensitizer manifesting near-infrared luminescence.

1 Introduction

Singlet oxygen ($^1\text{O}_2$), the first excited state $^1\Delta_g$ of molecular oxygen, is a highly reactive species which plays an important role in a wide range of biological processes, *e.g.* cell signalling, immune response, macromolecule degradation, or elimination of neoplastic tissue during photodynamic therapy (PDT). Probably the most important way of $^1\text{O}_2$ production is the photosensitizing process, where a molecule of a photosensitizer (PS) is excited by light and forms the triplet state by inter-system crossing, which can afterwards collide with ground state oxygen $\text{O}_2(^3\Sigma_g^-)$ giving rise to $^1\text{O}_2$. $^1\text{O}_2$ exhibits a very weak near-infrared (NIR) phosphorescence band around 1275 nm (with quantum yield of $\approx 6.5 \times 10^{-7}$ in water¹), which allows for its direct detection. $^1\text{O}_2$ phosphorescence-based microscopy of cells containing either exogenous or endogenous PSs would be an invaluable tool for research in fields of PDT or antioxidants. Although there have been a significant progress achieved especially by Ogilby's group about 10 years ago²⁻⁴, $^1\text{O}_2$ luminescence microscopy on the cellular and sub-cellular level still remains a big challenge. The recent introduction of improved NIR-sensitive 2D arrays is about to bring a renaissance into this field.

Given the very poor quantum yield of $^1\text{O}_2$ phosphorescence, a remarkable effort have been put into the development of indirect methods of $^1\text{O}_2$ detection and imaging. Among

others, Singlet Oxygen Sensor Green[®] (SOSG) fluorescent probe has been used for imaging of $^1\text{O}_2$ production *in vivo* in plant leaves subjected to photo-oxidative stress⁵ or for microscopy of individual living cells⁶. However, due to endogenous $^1\text{O}_2$ production from the probe itself, this technique lacks specificity^{7,8}. A different approach was implemented by Mosinger *et al.*: Singlet oxygen-sensitized delayed fluorescence (SOSDF), where the PS itself acts as a $^1\text{O}_2$ probe, was employed for imaging of $^1\text{O}_2$ generation in polymeric nanofibers loaded with tetraphenylporphyrin⁹. The phenomenon of SOSDF has recently been observed in our lab in solutions of a wide range of water-soluble $^1\text{O}_2$ PSs and SOSDF thus seems to be a potentially promising indirect method for microscopy of biological systems^{10,11}. Although the indirect methods generally exhibit much stronger signals than $^1\text{O}_2$ phosphorescence, they bear obvious disadvantages as an inhomogeneous spatial distribution of the probe in a cell and its non-perfect specificity to $^1\text{O}_2$. Therefore, $^1\text{O}_2$ phosphorescence-based microscopy is still irreplaceable.

Several papers on direct $^1\text{O}_2$ -based imaging of tumors during PDT using either a 2D detector array or a scanning approach have been published¹²⁻¹⁴. In the field of microscopy, the group of Ogilby managed to acquire nice images of $^1\text{O}_2$ phosphorescence from individual nerve cells loaded with TMPyP²⁻⁴. However, as only a 1D array detector was available, the sample had to be scanned line by line, which led to a prolonged acquisition and exposure time in the range of several minutes and uneven photobleaching across the acquired image.

The aim of the work is to present our new setup using a novel 2D array InGaAs detector NIRvana: 640 from Princeton Instruments, to evaluate its imaging ability, and to demonstrate $^1\text{O}_2$ -based microspectroscopy images of individual cells. The new 2D detector, which is now commercially available, allowed us to shorten the acquisition time of $^1\text{O}_2$ -based images substantially to ~ 5 s with respect to older work by Ogilby *et al.* An imaging spectrograph inserted in front of the 2D-array detector allows us to acquire spectral images where one dimension is spatial and the other is spectral. Our methodology of acquiring spectral images of individual cells provides a foundation for separation of $^1\text{O}_2$ phosphorescence from spectrally overlapping NIR-extended luminescence of the PS, which otherwise may be a persistent problem for a number of different photosensitizers. TMPyP is used as a photosensitizer throughout the work in order to relate to older work of Ogilby's group^{2-4,15} and other numerous papers on luminescence microscopy and spectroscopy of TMPyP in mammalian cells^{16,17}. Moreover, the NIR-extended luminescence of TMPyP^{10,18} manifests the necessity of spectral images for distinguishing between PS and $^1\text{O}_2$ luminescence.

^a Charles University in Prague, Faculty of Mathematics and Physics, Department of Chemical Physics and Optics, Ke Karlovu 3, 121 16 Praha 2, the Czech Republic. Fax: +420221911249; Tel: +420221911248; E-mail (M. Scholz): marasolc@centrum.cz

^b University of Aarhus, Department of Chemistry, Center for Oxygen Microscopy and Imaging, Langelandsgade 140, 8000 Aarhus, Denmark.

2 Experimental

The experimental setup is schematically represented in Fig. 1. It is built around an inverted fluorescence microscope (IX71, Olympus). The excitation beam provided by the 405 nm CW laser (LDM405.120.CWA.L, Omicron) is passed through ND filters and coupled into the NIR-corrected objective OBJ (LM-Plan IR, 50x/0.55, Olympus) by the 500 nm dichroic longpass mirror DLP (Edmund Optics). The lens L1 ($f=50$ mm, Thorlabs) is inserted into the excitation path to enlarge the illuminated spot on the sample S (*i.e.*, shifting the laser focal plane out of the sample focal plane). The diameter of the illuminated area on the sample is 94 μm . The laser power density at the sample usually varied from 1 W/cm^2 to 5 W/cm^2 depending on the specific experiment. The luminescence emission from the sample collected by the objective passes through the dichroic mirror DLP and is either directed by the golden mirror GM (Edmund Optics) to the NIR detection path or by sliding the GM out passed to the VIS detection path. In the NIR path, the signal is passed through a combination of NIR longpass and shortpass filters F depending on the specific experiment (longpass 850 nm and 1100 nm, shortpass 1100 nm Edmund Optics; longpass 1250 nm and 1350 nm Thorlabs) and then focused by lens L2 (achromatic, $f=20$ cm, Edmund Optics) on the entrance slit of the imaging spectrograph (Acton SpectraPro 2500i, Princeton Instruments) which is coupled to a NIR-sensitive InGaAs camera (NIRvana:640, Princeton Instruments) cooled to -80°C . The spectrograph was used either with a grating (150 g/mm , 1.2 μm blazed) for spectroscopy or with a mirror for imaging. The shutter SH in the excitation path controlled by the camera is opened only in the period of exposure to minimize the photobleaching of the sample. In the imaging mode, the pixel size of the NIRvana camera $20 \times 20 \mu\text{m}$ corresponds to area of $0.34 \times 0.34 \mu\text{m}$ on the sample as determined from the $58\times$ magnification of the system. At 1275 nm ($^1\text{O}_2$ phosphorescence band), the spatial resolution due to the diffraction limit is $\approx 1.4 \mu\text{m}$ according to the Rayleigh criterion as determined by objective numerical aperture of 0.55. Therefore, 2×2 binning was performed to meet the Nyquist sampling theorem. In the spectroscopy mode, the spectral resolution of the system was 10 nm as defined by the width of the entrance slit of the spectrograph. The VIS detection path is realized analogically by a VIS sensitive back-illuminated silicon camera (Spec-10:400B, Princeton Instruments) coupled to the imaging spectrograph (Acton SP 2300i, Princeton Instruments). During recent further improvements the golden mirror GM was replaced by a 1000 nm shortpass dichroic mirror DM (Thorlabs) to enable simultaneous detection in the VIS and NIR spectral regions, and the set of filters F was completed by 1274/40 nm and 1200/40 nm bandpass filters (Omega Optical) with peak transmission $> 70\%$.

The 3T3 mouse fibroblasts (ATCC: CCL 92, cultured as described in¹⁷) were seeded out to half confluence into dishes (μ -Dish 35mm, glass bottom, IBIDI) one day before the incubation. The cell samples for the imaging experiments have been prepared by three different incubation procedures:

P1) Incubation according to the procedure applied to neurons described by Ogilby *et al.*², which includes replacement of intracellular H_2O with D_2O in order to increase the

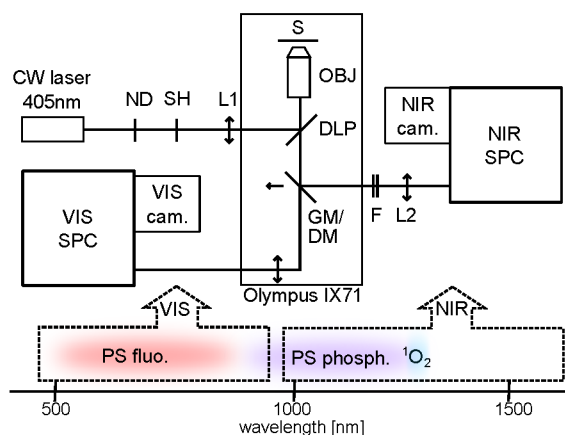


Fig. 1 The scheme of the setup for NIR luminescence microspectroscopy. The bottom part of the figure schematically shows the spectral regions detected by VIS and NIR path, respectively. Detailed description is provided in the text.

$^1\text{O}_2$ lifetime. Briefly, the monolayer of cells covering the dish was washed properly with a D_2O -based saline solution and treated with a hypertonic D_2O -based saline solution for 5 minutes. Then the cells were incubated for 5 hours in an isotonic D_2O -based saline solution with 100 μM 5,10,15,20-tetrakis(1-methyl-4-pyridinio)porphine (TMPyP^{4,16,19}) and washed properly with an isotonic D_2O -based saline solution afterwards to remove the extracellular TMPyP.

P2) Analogically to the procedure P1, but the cells were incubated for 20 hours.

P3) An aliquot of 100 μM TMPyP was added into growth medium and the sample was incubated for 20 hours^{16,17}, then H_2O was replaced with D_2O (as described above) and the sample was kept in D_2O -based saline solution for 1 h.

In all the cases, the cell samples were held under oxygen atmosphere during the experiments. Most of the experiments were carried out with cells prepared according to the procedure P1. Experiments demonstrating NIR spectral changes during irradiation (Fig. 4-A) were performed with cells incubated according to P2, which show substantially increased retention of TMPyP while they still maintain their shape as demonstrated by the fluorescence image. The incubation according to P3 minimizes the stress imposed on the cells compared to the latter two procedures but generally produces a weaker signal. Trypan blue staining test provided viabilities of the cells $> 85\%$, $< 10\%$, and $> 95\%$ for procedures P1, P2, and P3, respectively.

Trypan blue exclusion assay for testing the cell membrane integrity: Monolayer of the cells in the dish was washed with neat PBS and then treated for five minutes with 0.4% Trypan blue solution (Sigma-Aldrich) diluted four-fold in PBS. The cells were washed again with neat PBS afterwards and the monolayer was inspected using bright field microscopy. Dead cells are stained by trypan blue while the cells with intact membranes are not.

3 Results and discussion

3.1 Sensitivity and noise characteristics of the setup

The ability of the system to detect $^1\text{O}_2$ was first tested by measuring NIR spectra of air-saturated solutions of several porphyrin-based PSs. The spectra featured a typical $^1\text{O}_2$ band around 1275 nm which was quenched in nitrogen-saturated samples or sodium azide (NaN_3 , 10 mM) containing samples (data not shown). In order to estimate the $^1\text{O}_2$ -detection efficiency, a 0.1 mm pathlength cuvette filled with 200 μM solution of tetraphenylporphyrin (TPP) in benzene was used as a sample on the microscope stage. Quantum yield of $^1\text{O}_2$ production ($\Phi_{\Delta} = 0.65 \pm 0.15^{20}$) and quantum yield of $^1\text{O}_2$ phosphorescence ($\Phi_{\text{ph}} = 4.7 \pm 1.7 \times 10^{-5} \text{ }^{1,21}$) are well documented for TPP in benzene. A combination of 1100 nm and 1250 nm longpass filters was used in the detection path and the spectrograph was set to imaging mode. By measuring the spectra, it was verified that $> 90\%$ of the emission is indeed due to $^1\text{O}_2$ phosphorescence.

In the limit of weak excitation laser power, the number of $^1\text{O}_2$ -phosphorescence photons N emitted from the laser excited volume per second can be determined as

$$N = \frac{P(1 - 10^{-A})\Phi_{\Delta}\Phi_{\text{ph}}}{h\nu}, \quad (1)$$

where P is the excitation laser power, $h\nu$ photon energy, and $A = 0.23$ absorbance of the sample at the wavelength of the laser. The total number of signal counts on the detector divided by the number N of emitted $^1\text{O}_2$ -phosphorescence photons gives the detection efficiency η of the whole setup. Fig. 2 shows the dependence of the apparent η value on the decreasing excitation power. The decrease of the apparent η values at higher excitation powers can be explained by saturation and/or local photobleaching of the PS. The real detection efficiency η of the setup was estimated by extrapolation of the apparent η value to zero excitation power. The applied experimental method provides a lower limit for the detection efficiency η (e.g. due to sample thickness larger than the depth of field of the imaging system) and therefore it can be concluded that $\eta \gtrsim 1\%$. The luminescence collection efficiency of the objective with N.A. = 0.55 is $\eta_1 = 8.2\%$ for isotropic emitter (which is the case of $^1\text{O}_2$). The transmission efficiency of the rest of the detection path is $\eta_2 = 45\%$ as determined by transmissions of individual optical elements. The relatively complicated setup with spectrograph requires us to be very careful when choosing optical elements with optimal performance. The quantum efficiency of the NIRvana camera is stated to be $\eta_3 = 85\%$ by the manufacturer. The theoretical detection efficiency $\eta' = \eta_1\eta_2\eta_3 = 3.1\%$ represents the upper limit and thus it can be concluded that the quantum efficiency of the setup is 1 – 3%. It is obvious that there is still a plenty of room for improvement, the objective being the most limiting element.

The dark noise of the NIRvana detector cooled to -80°C was determined in the following experiment: Sequences of twenty frames were acquired for a range of exposure times per frame (1 ms - 25 s), the detector being in dark (attached to a spectrograph with entrance slit closed; spectrograph being at

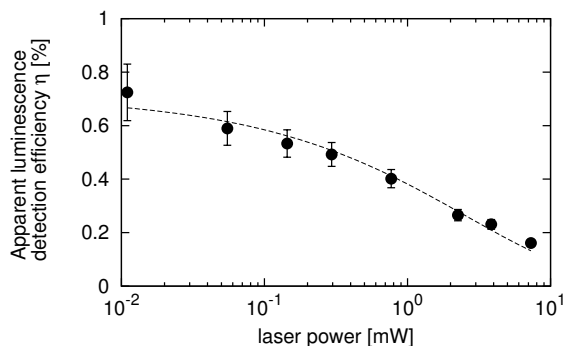


Fig. 2 The apparent luminescence detection efficiency η in dependence on the laser excitation power. The data were fitted by a stretched exponential function.

room temperature in a dark room). The values of dark counts per pixel in Fig. 3 were obtained as a mean number of counts per pixel in the averaged sequence of dark frames. Neither background nor flat-field correction were used. The principal sources of dark counts are i) readout of the detector and ii) darkcurrent - a thermally induced buildup of dark charge over time. Dark counts values can be fitted as a linear function of exposure time. The slope of the line (350 counts/s/pixel) corresponds to darkcurrent and matches the value provided by the manufacturer in the detector specification, whereas the y-axis intercept is related to the readout. The DC level of the dark counts is not uniform over the detector, but applying background correction can easily remove the bias pattern in the image. Therefore, the noise level is determined by standard deviation of dark counts in individual pixels. In every pixel of the detector, the standard deviation of dark counts across the sequence of frames was determined. The mean value of the standard deviation over all the pixels in the detector is displayed in Fig. 3*. The values of standard deviation roughly correspond to the square root of the DC level of dark counts, *i.e.* revealing properties of the Poisson distribution, as expected. The standard deviation of dark counts per pixel (*i.e.* the dark noise level) of the detector cooled down to -80°C was found to be 130 counts per pixel in 5 s (260 counts if 2×2 -binning applied). The readout noise corresponding to standard deviation of dark counts at a very short exposition of 1 ms (115 counts per pixel with no significant dependence on readout speed) is obviously the main constituent of the overall noise. Therefore, if a decreased time resolution is not a concern, it can be more convenient to use one longer exposure instead of several shorter ones. The manufacturer states that exposure times up to 1-2 minutes are possible. Together with the detection efficiency of the setup this provides a framework for evaluation whether the $^1\text{O}_2$ -based image of a particular sample can be detected. Further reference on the characterization of noise and sensitivity of imaging systems and detectors can be found in numerous publications²²⁻²⁵.

Let us consider the following calculation: The 2×2 binned pixel corresponds to an area of $S = 0.68 \times 0.68 \mu\text{m}^2$ on the

* Standard deviation calculated for a difference image²² – difference between two images with the same exposure time – provides similar results.

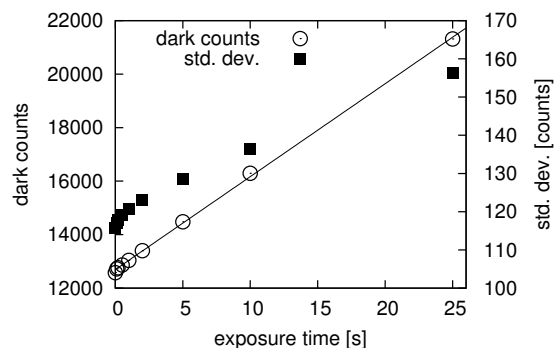


Fig. 3 Dark counts per pixel and its standard deviation for different exposure times per frame.

sample. Assuming that we observe a mammalian cell with a thickness of $w \approx 5 \mu\text{m}$, the volume from which the signal is collected to the 2×2 binned pixel is $V = 2.3 \text{ fl}$. If the acquisition time is $t = 5 \text{ s}$, the noise-equivalent signal is $s = 260$ counts per 2×2 binned pixel. The concentration of $^1\text{O}_2$ providing the noise-equivalent signal in the 2×2 binned pixel in acquisition time t is then

$$[^1\text{O}_2] = \frac{s}{\eta t k_{\text{ph}} V N_{\text{A}}} = 18 \mu\text{M}, \quad (2)$$

where $k_{\text{ph}} \approx 0.2 \text{ s}^{-1}$ is the radiative rate of $^1\text{O}_2$ in D_2O , $\eta = 1\%$, and N_{A} Avogadro constant. The corresponding concentration of TMPyP in D_2O -treated cells can also be estimated. Irradiation power per unit of area I_{A} absorbed by the TMPyP-loaded cell monolayer meets the following equation

$$I_{\text{A}} = \frac{s \hbar \omega}{\eta \Phi_{\text{ph}} \Phi_{\Delta} s t} \approx 0.23 \text{ W/cm}^2, \quad (3)$$

where $\hbar \omega$ is the photon energy, $\Phi_{\Delta} \approx 0.4$ quantum yield of $^1\text{O}_2$ in cellular environment¹⁶, and $\Phi_{\text{ph}} = k_{\text{ph}} \tau_{\Delta} \approx 6 \times 10^{-6}$ phosphorescence quantum yield of $^1\text{O}_2$ using lifetime of $^1\text{O}_2$ in a cell $\tau_{\Delta} \approx 30 \mu\text{s}$ ^{16,26}. In the approximation of the Lambert-Beer law, the absorbance of the sample $A = \log(1 - I_{\text{A}}/I_0) = 0.11$ for $I_0 = 1 \text{ W/cm}^2$. The concentration of TMPyP in the monolayer of cells is then

$$[\text{TMPyP}] = \frac{A}{\varepsilon w} = 1.1 \text{ mM} \quad (4)$$

where $\varepsilon \approx 2 \times 10^5 \text{ M}^{-1} \text{ cm}^{-1}$ is the absorption coefficient of TMPyP at its maximum. This is a conceivable concentration of the PS accumulated in a cell¹⁶, although it has to be remembered that it is only an estimate as many of the used parameters may depend on various factors, such as oxygen saturation, excitation intensity *etc.*

The $^1\text{O}_2$ -detection ability of the NIRvana camera and the older custom-made InGaAs 1D-array detector²⁷ used by Ogilby's group were compared using the same excitation intensity and air-saturated solution of TMPyP in D_2O -based PBS as a sample. The data indicate that the signal-to-noise ratio is somewhat larger ($1.6 \pm 0.6 \times$) for NIRvana detector. Nevertheless, the main advantage of the NIRvana camera compared to the older 1D-array is the ability to acquire

the image all at once without scanning, which dramatically reduces acquisition time and also eliminates the problem of gradual photobleaching during the scanning process (*i.e.* in the case of 1D-array scanning approach, every strip of the resulting scanned image is acquired in a different time and different stage of photobleaching^{3,4}).

3.2 Overlap of luminescence of singlet oxygen and photosensitizer in cells

Fig. 4-A displays the cell sample incubated with $100 \mu\text{M}$ TMPyP for 20 h in D_2O -based saline solution (incubation procedure P2). At the beginning, the bright field image, visible fluorescence image, and the fluorescence spectrum were acquired. Then ten consecutive frames of 5 s of NIR spectral images were acquired using continuous excitation with power density of 5 W/cm^2 and combination of 850 nm longpass and 1100 nm longpass emission filters. Spectral images are collected from the region defined by the entrance slit of the spectrograph (green rectangle in the Fig. 4-A: image > 1250 nm), their vertical dimension being spatial whereas the horizontal dimension is spectral. The detected spectra obtained by vertical binning of the spectral images are shown at three selected times (5 s, 30 s, 50 s). The characteristic $^1\text{O}_2$ phosphorescence band around 1275 nm is clearly visible. The broad-band signal overlapping with $^1\text{O}_2$ phosphorescence, which is due to the tail of the PS luminescence, bleaches much faster than the $^1\text{O}_2$ phosphorescence itself (discussed hereinafter). Therefore, after 50 s irradiation the $^1\text{O}_2$ band becomes prominent and free of the broad-band background. Afterwards, the image of $^1\text{O}_2$ phosphorescence was acquired with 10 s exposition using a combination of 850 nm and 1250 nm longpass filters. Then the sample was left in dark for 5 minutes and the liquid surrounding the cells was stirred very gently. No change in the sharpness of the NIR and VIS luminescence images was observed. Moreover, the intensity of >1250 nm emission slightly increased and there was no reappearance of the broad-band background. This indicates that the signal originated inside the cells and that no substantial leakage of the PS out from the cell occurred. The increased intensity may be explained by the recovery of oxygen concentration inside the cells after its depletion during irradiation. Furthermore, the fluorescence spectrum before and after the experiment were compared. Apart from the lowered intensity, a slight change of the spectral shape can be observed (the longer-wavelength band being relatively weaker). The distribution of the fluorophore inside the cells also slightly differs as was observed from fluorescence images before and after (data not shown). These observations are in line with previously reported relocation of TMPyP within the cell during irradiation^{4,15,28,29}. Finally, the 1275 nm spectral band was quenched by addition of 10 mM NaN_3 , a specific $^1\text{O}_2$ quencher, which further supports that the 1275 nm band can indeed be identified with $^1\text{O}_2$ phosphorescence. The $^1\text{O}_2$ band is quenched by NaN_3 also in a fresh sample (prior to irradiation), contrary to the broad-band background, which is not quenched (data not shown). No distinct $^1\text{O}_2$ phosphorescence band appeared in H_2O -treated samples which is in line with expectations, as H_2O is a much more potent $^1\text{O}_2$ -deactivator than D_2O and it was also shown to be the

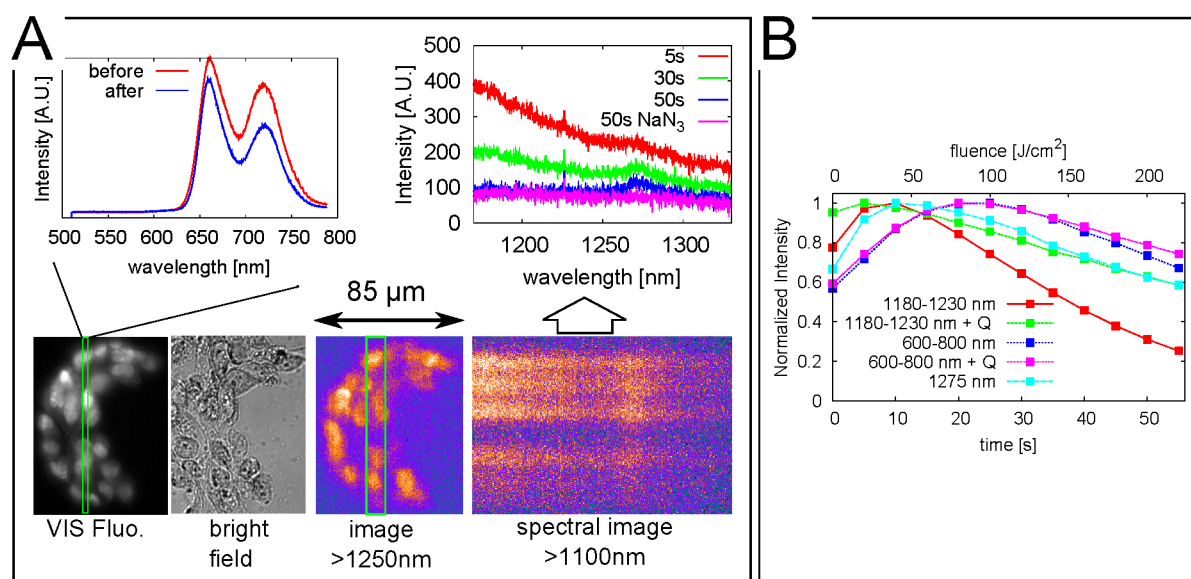


Fig. 4 A: NIR luminescence based images and spectra accompanied by bright-field and VIS fluorescence-based images of 3T3 mouse fibroblasts incubated for 20 h with 100 μM TMPyP in D_2O -based saline solution (incubation procedure P2). The green rectangles are defined by the entrance slit of the spectrographs and represent the area where the spectral images are collected from. The graphs of spectra were obtained by vertical binning of the spectral images. Further description is provided in the text. B: Changes of luminescence intensity in three different spectral regions during the course of irradiation. Q denotes that the sample contained a $^1\text{O}_2$ quencher (NaN_3 or H_2O).

major quencher of $^1\text{O}_2$ in cells²⁶.

Fig. 4-B demonstrates how the luminescence signal changes during the course of irradiation in the cell samples incubated according to the procedure P2. The signal was measured in three different spectral regions – 600-800 nm (VIS fluorescence of PS), 1180-1230 nm (NIR luminescence of PS), and 1250-1300 nm ($^1\text{O}_2$ emission). The VIS fluorescence signal shows rise at the beginning, which is in line with older observations⁴. The broad NIR background luminescence of PS clearly bleaches faster than the $^1\text{O}_2$ emission. The bleaching of NIR luminescence of PS is slowed down when a specific $^1\text{O}_2$ quencher is added. This suggests that the bleaching is at least partly caused by oxidation due to $^1\text{O}_2$. The bleaching of VIS fluorescence is not substantially influenced by presence of $^1\text{O}_2$ quenchers. The $^1\text{O}_2$ quencher can be either NaN_3 , or D_2O can be replaced with H_2O which also dramatically reduces $^1\text{O}_2$ lifetime. The displayed kinetics were averaged over five normal samples and five $\text{NaN}_3/\text{H}_2\text{O}$ -treated samples.

The NIR broad-band background luminescence of TMPyP appears also in bulk solutions of TMPyP in D_2O (concentration range 100-500 μM), as demonstrated in Fig. 5. The solutions were placed into 1 mm pathlength cuvette on the microscope stage. Interestingly, in a concentrated sample (500 μM TMPyP) at strong excitation intensities (9 W/cm^2) the NIR broad-band background is enhanced and $^1\text{O}_2$ phosphorescence is suppressed, whereas using a weaker excitation 2.5 W/cm^2 at the same concentration leads to a recovery of $^1\text{O}_2$ phosphorescence and decrease of the NIR broad-band background.[†] The displayed spectral image of this sample also

demonstrates that the 1170 – 1200 nm emission is confined to the region where the excitation is strongest, whereas $^1\text{O}_2$ phosphorescence is emitted also from weakly excited regions (this cannot be due to $^1\text{O}_2$ diffusion because the diffusion length is $< 1 \mu\text{m}$ ^{16,26}). These observations indicate that the NIR broad-band background luminescence is enhanced when the concentration of excited states is larger, suggesting that an excited state reaction or excited state complex formation takes place. For each concentration, there is an optimal excitation intensity to achieve maximal $^1\text{O}_2$ phosphorescence signal and contrast. Too large excitation power or PS concentration may actually lead to signal suppression. This conclusion could be extended also to the cell samples loaded with TMPyP, where the local TMPyP concentration can be relatively large (millimolar range for living human skin fibroblasts incubated with 100 μM TMPyP¹⁶). Therefore, an optimal excitation intensity has to be chosen carefully for each sample according to the PS concentration.

The spectral changes during irradiation of the cell samples shown in Fig. 4 could be partly explained by reduction of the local TMPyP concentration due to photobleaching (as discussed in the previous paragraph). However, the full explanation is probably far more complicated. An interplay of several additional factors, such as formation of TMPyP-photoproduct(s) with reduced NIR emission still producing $^1\text{O}_2$ or TMPyP relocation to different cell compartments^{4,15,28,29}, is likely to be manifested. The NIR broad-

sample) as the excitation power was being decreased. At the end (with the same sample), the excitation power was increased again and a spectral image was acquired. Then, with a fresh sample, a series of spectral images for increasing excitation powers was acquired as a control experiment. Analogous experiments were carried out several times with consistent results.

[†] The experiment with different excitation intensities was conducted in the following way: First, a series of spectral images was acquired (with the same

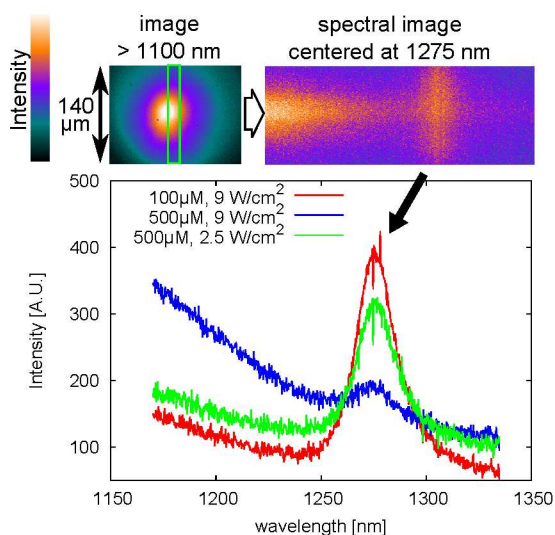


Fig. 5 NIR spectra taken from TMPyP solutions of two different concentrations under diverse excitation powers. A 1 mm cuvette containing the solution was placed on the microscope sample stage. The green rectangle is defined by the entrance slit of the spectrograph and represents the area where the spectral image was collected from. The graph of the spectrum was obtained by vertical binning of the spectral image.

band background was observed in cells loaded with TMPyP from three different suppliers (Porphyrin Systems, Frontier Scientific, and Sigma-Aldrich) and was not observed in a sample without TMPyP, which proves that autofluorescence can be excluded and that an effect of impurity is improbable.

3.3 Separation of singlet oxygen image from the background luminescence of photosensitizer in cells

As it was demonstrated in the previous section, the NIR tail of TMPyP luminescence can spectrally overlap with $^1\text{O}_2$ phosphorescence. The following section shows $^1\text{O}_2$ -based images of cells and discusses the possible ways of separation of $^1\text{O}_2$ signal from NIR luminescence of the PS.

Fig. 6-A displays the images of a cell incubated for 5 h with 100 μM TMPyP in D_2O -based saline solution (incubation procedure P1). Ten consecutive frames of 5 s were acquired using continuous 1 W/cm^2 irradiation. The image >1250 nm (combination of 850 and 1250 nm longpass filters) is the sum of the last four frames (*i.e.* 20 s exposition). Subsequently, the spectral image was obtained with 25 s exposition. The bright-field and fluorescence images were taken afterwards. The spectrum shows that $^1\text{O}_2$ phosphorescence is the dominant spectral feature. Additionally, it was verified for other cells that the intensity of the >1250 nm image drops by more than 70% when the 1250 nm longpass filter is replaced by a 1350 nm longpass filter.

Fig. 6-B displays another sample of cells incubated according to the procedure P1. Four near-infrared images were taken using 2.5 W/cm^2 irradiation. First the 850–1100 nm image (I_1 , combination of 850 nm longpass and 1100 nm shortpass

filters) was acquired with 1 s exposition. Subsequently the >1250 nm image (I_2) was taken with 5 s exposition. Then the aliquot of 10 mM NaN_3 was added to the sample and this was gently stirred and left in dark for 5 minutes. Afterwards, the 850–1100 nm image (I_3) with 1 s exposition and the >1250 nm image (I_4) with 5 s exposition were acquired again. A slight drop in the 850–1100 nm signal can be observed, which is probably indicating a certain level of photobleaching. However, much stronger drop of signal after addition of NaN_3 is seen in the case of the >1250 nm image (I_4). The $^1\text{O}_2$ signal is assumed to be almost completely quenched in the I_4 image - this is formed mainly by the NIR background luminescence of TMPyP. The $^1\text{O}_2$ -based image ($R_{1\text{O}_2}$) can be then reconstructed by subtracting I_4 from I_2 . Moreover, the I_4 image can be corrected by factor I_1/I_3 in order to compensate for the photobleaching of the NIR background luminescence of TMPyP during the irradiation:

$$R_{1\text{O}_2} = I_2 - I_4 \frac{I_1}{I_3}.$$

Such reconstructed image thus shows only the portion of the signal which is quenched by NaN_3 , *i.e.* $^1\text{O}_2$ signal. The bright-field and fluorescence images are shown for comparison.

The cells prepared according to the procedures P1 and P2 were significantly perturbed during the sample preparation by changing to D_2O -based medium and by the absence of growth medium. Unperturbed cells exhibited much smaller uptake of the PS leading to a very weak signal. In order to test the cell membrane integrity of the cells, trypan blue exclusion test was performed. Although the viability of the cells prepared according to the procedure P1 was found to be $> 85\%$ as determined by trypan blue test, it was observed that TMPyP was preferentially uptaken into trypan blue-stained dead cells. Both TMPyP and trypan blue are positively charged water-soluble molecules which accumulate in the nucleus due to their high affinity to DNA. In order to prove that we are able to detect $^1\text{O}_2$ also from intact cells which are negative in trypan blue test, we stained the sample with trypan blue before the luminescence experiment. After washing out properly any residual trypan blue stain, the sample was placed into the luminescence microscope and the luminescence was measured selectively from trypan blue-unstained cells. This is demonstrated in Fig. 7. The samples were irradiated by 2.5 W/cm^2 . Sample 1 and 2 were first exposed for 30 s to obtain the $^1\text{O}_2$ -based image and then for 50 s and 20 s, respectively, to obtain the spectral image. The VIS fluorescence intensity dropped by $\approx 75\%$ and $\approx 50\%$, respectively, during the experiments. The NIR spectrum and spectral images clearly manifest a spectral band around 1275 nm corresponding to $^1\text{O}_2$. NIR luminescence of TMPyP is also present reaching a similar intensity around 1200 nm. Various researches have been using ~ 1270 nm and 1200 nm bandpass filters in their experiments to demonstrate that there is an emission around 1270 nm but not around 1200 nm, thus proving that $^1\text{O}_2$ is the emitting species^{2,30,31}. Nevertheless, both ~ 1270 nm and ~ 1200 nm images would provide similar intensities in this case, which is shown in Fig. 8. The cells were incubated for 20 h with 100 μM TMPyP in growth medium (incubation procedure P3),

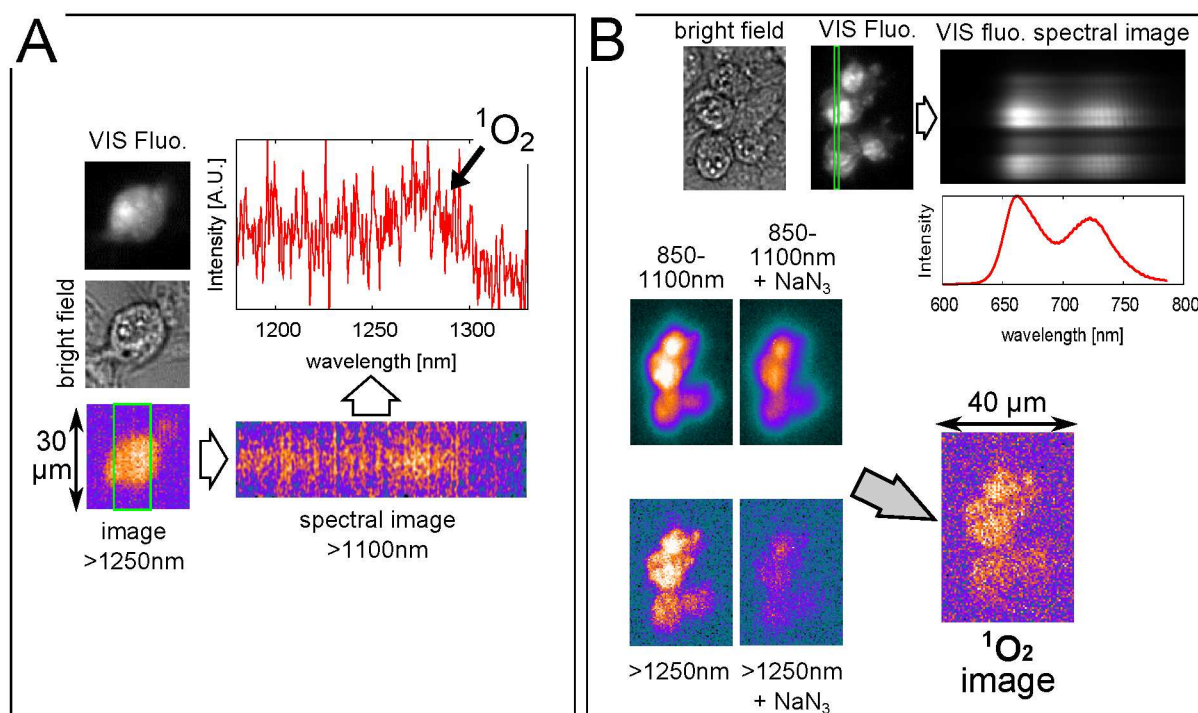


Fig. 6 NIR luminescence based images and spectra accompanied by bright-field and VIS fluorescence-based images of 3T3 mouse fibroblasts incubated for 5 h with 100 μM TMPyP in D_2O -based saline solution (incubation procedure P1). Frames A and B represent two different samples. The green rectangles are defined by the entrance slit of the spectrographs and represent the areas where the spectral images are collected from. The graphs of spectra were obtained by vertical binning of the spectral images. Gaussian blur filter with unit radius (ImageJ image processing software) was applied to smooth the spectral image in order to make the weak spectral features more distinguishable.

which minimizes the stress imposed on the cells in comparison with the other two methods, but usually provides a weaker signal (here collected for one minute using irradiation power of 2.5 W/cm^2). Generally, if the NIR luminescence of a photosensitizer extends to the wavelengths $> 1200 \text{ nm}$, the control experiment using a 1200 nm bandpass filter may still provide an appreciable signal and, at the same time, it may be impossible to quench completely the signal around 1275 nm by a $^1\text{O}_2$ quencher. This demonstrates the benefits of spectral images over bandpass filter method for distinguishing $^1\text{O}_2$ luminescence. It will be even more pronounced in the case of H_2O -incubated cell samples, where the $^1\text{O}_2$ signal will be further suppressed compared to the NIR-extended luminescence of a photosensitizer.

Naturally, the overall aim is to provide $^1\text{O}_2$ images of healthy unperturbed cells in their native H_2O -based environment. To this end, further development of the methodology is required (selection of the most appropriate PS, higher numerical aperture objective, optimization of the procedure of cell incubation, irradiation intensity, exposure time, magnification *etc.*). The use of TMPyP as a sensitizer for $^1\text{O}_2$ -based microscopy conceals several obstacles. It was shown that the irradiation intensity and/or loading concentration has to be properly chosen to maximize the $^1\text{O}_2$ luminescence signal and minimize the TMPyP near-infrared luminescence signal. As a water-soluble cationic photosensitizer, TMPyP was observed to accumulate preferentially in the cells with perturbed membranes. Another photosensitizers, possibly lipid-soluble ones,

should be considered for further experiments.

4 Conclusions

In conclusion, our setup employing the novel NIR-sensitive 2D-array InGaAs detector (NIRvana) proved to be sensitive enough to provide $^1\text{O}_2$ images of individual D_2O -treated fibroblast cells incubated with TMPyP. The overall efficiency of $^1\text{O}_2$ phosphorescence detection was estimated to be 1 – 3%, the numerical aperture of the objective (N.A. = 0.55) being the main limiting factor. The main advantage of the new detector over the 1D-array InGaAs detector used earlier by the Ogilby's group^{2,3} is its two-dimensionality, which leads to a dramatic reduction of acquisition times and avoids some of the problems caused by photobleaching of the sample. Two detection channels (VIS and NIR) allow us to perform a real-time imaging of the very weak near-infrared phosphorescence of $^1\text{O}_2$ and PS simultaneously with visible fluorescence of the PS. Moreover, our new setup enables us to obtain spectral images based on $^1\text{O}_2$ and PS luminescence from individual cells, where one dimension of the image is spatial and the other is spectral, allowing to cover a wide spectral range from 500 nm to 1700 nm. To our knowledge, this is the first report in this respect. By acquiring a time-development of near-infrared spectral images of $^1\text{O}_2$ and PS luminescence during irradiation of individual TMPyP-loaded cells, TMPyP was found to exhibit rather complicated spectral properties with near-

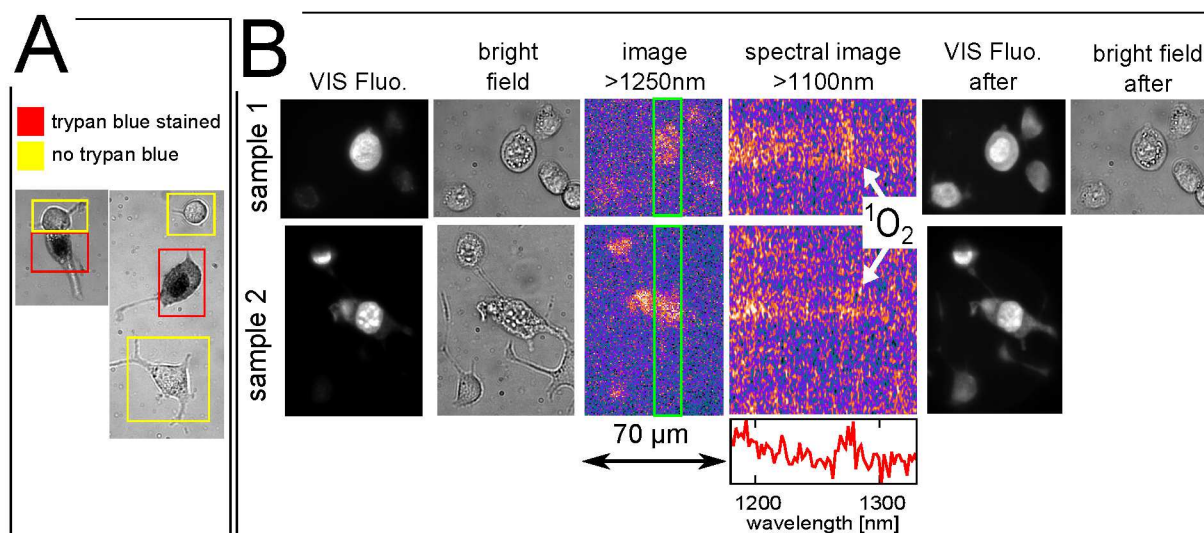


Fig. 7 A: The difference between trypan blue-stained and -unstained cells in bright field. B: NIR luminescence based images and spectra accompanied by bright-field and VIS fluorescence-based images of 3T3 mouse fibroblasts incubated for 5 h with 100 μM TMPyP in D₂O-based saline solution (incubation procedure P1). Trypan blue-unstained cells were selectively chosen for the experiment. To obtain the bright-field images in experiments A and B, the samples were illuminated by a lamp through a 600 nm/40 nm bandpass filter in order to enhance the trypan blue contrast. Gaussian blur filter with unit radius (ImageJ image processing software) was applied to smooth the spectral images in order to make the weak spectral features more distinguishable.

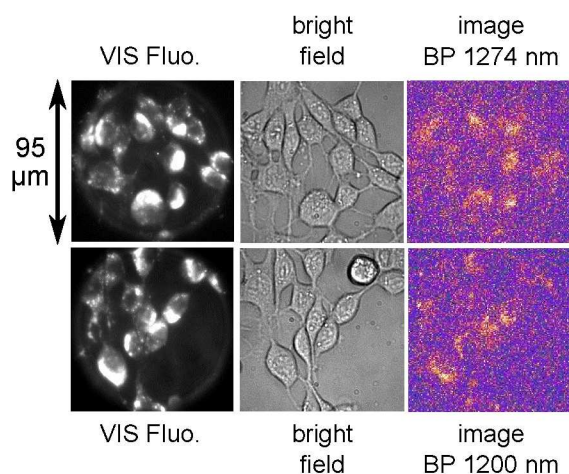


Fig. 8 NIR luminescence based images (using either 1274/40 nm or 1200/40 nm bandpass filters) accompanied by bright-field and VIS fluorescence-based images of 3T3 mouse fibroblasts. The cells were incubated for 20 h with 100 μM TMPyP in growth medium and subsequently H₂O was replaced with D₂O (incubation procedure P3).

infrared emission extending to the wavelengths corresponding to $^1\text{O}_2$ phosphorescence. The NIR spectral images provide a basis for distinguishing and separation of $^1\text{O}_2$ phosphorescence from NIR luminescence of a PS, which may spectrally overlap for a number of PSs. Further development of the technique is needed if we aim to provide images of $^1\text{O}_2$ phosphorescence from unperturbed living cells in their natural environment without performing a $\text{H}_2\text{O}-\text{D}_2\text{O}$ exchange.

Acknowledgements: The work was supported by project number 848413 from the Grant Agency of Charles University and project P501/12/G055 from the Czech Science Foundation.

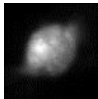
References

- C. Schweitzer and R. Schmidt, Physical mechanisms of generation and deactivation of singlet oxygen., *Chem. Rev.*, 2003, **103**, 1685–1757.
- I. Zebger, J. W. Snyder, L. K. Andersen, L. Poulsen, Z. Gao, D. C. John, U. Kristiansen, P. R. Ogilby and J. D. C. Lambert, Direct Optical Detection of Singlet Oxygen from a Single Cell, *Photochem. Photobiol.*, 2004, **79**, 319–322.
- J. W. Snyder, E. Skovsen, J. D. C. Lambert, L. Poulsen and P. R. Ogilby, Optical detection of singlet oxygen from single cells., *Phys. Chem. Chem. Phys.*, 2006, **8**, 4280–93.
- J. W. Snyder, J. D. C. Lambert and P. R. Ogilby, a Sensitizer for Singlet Oxygen Imaging in Cells : Characterizing the Irradiation-dependent Behavior of TMPyP in a Single Cellt, *Photochem. Photobiol.*, 2006, **82**, 177–184.
- C. Flors, M. J. Fryer, J. Waring, B. Reeder, U. Bechtold, P. M. Mullineaux, S. Nonell, M. T. Wilson and N. R. Baker, Imaging the production of singlet oxygen in vivo using a new fluorescent sensor, Singlet Oxygen Sensor Green., *J. Exp. Bot.*, 2006, **57**, 1725–34.
- Y. Shen, H. Lin, Z. Huang, D. Chen, B. Li and S. Xie, Indirect imaging of singlet oxygen generation from a single cell, *Laser Phys. Lett.*, 2011, **8**, 232–238.
- A. Gollmer, J. Arnbjerg, F. H. Blaikie, B. W. Pedersen, T. Breitenbach, K. Daasbjerg, M. Glasius and P. R. Ogilby, Singlet Oxygen Sensor Green: photochemical behavior in solution and in a mammalian cell., *Photochem. Photobiol.*, 2011, **87**, 671–9.
- X. Ragàs, A. Jiménez-Banzo, D. Sánchez-García, X. Batllori and S. Nonell, Singlet oxygen photosensitisation by the fluorescent probe Singlet Oxygen Sensor Green., *Chem. Commun.*, 2009, 2920–2.
- J. Mosinger, K. Lang, J. Hostomský, J. Franc, J. Sýkora, M. Hof and P. Kubát, Singlet oxygen imaging in polymeric nanofibers by delayed fluorescence., *J. Phys. Chem. B*, 2010, **114**, 15773–9.
- M. Scholz, R. Dēdic, T. Breitenbach and J. Hála, Singlet oxygen-sensitized delayed fluorescence of common water-soluble photosensitizers., *Photochem. Photobiol. Sci.*, 2013, **12**, 1873 – 1884.
- M. Scholz, R. Dēdic, J. Hála and S. Nonell, Oxygen effects on tetrapropylporphycene near-infrared luminescence kinetics, *J. Mol. Struct.*, 2012, **1044**, 303–307.
- B. Li, H. Lin, D. Chen, B. C. Wilson and Y. Gu, Singlet Oxygen Detection During Photosensitization, *J. Innov. Opt. Health Sci.*, 2013, **06**, 1330002.
- B. Hu, Y. He and Z. Liu, NIR area array CCD-based singlet oxygen luminescence imaging for photodynamic therapy, *J. Phys. Conf. Ser.*, 2011, **277**, 012011.
- M. J. Niedre, M. S. Patterson, A. Giles and B. C. Wilson, Imaging of Photodynamically Generated Singlet Oxygen, *Photochem. Photobiol. Sci.*, 2005, **81**, 941–943.
- E. F. F. da Silva, B. W. Pedersen, T. Breitenbach, R. Toftgaard, M. K. Kuimova, L. G. Arnaut and P. R. Ogilby, Irradiation- and sensitizer-dependent changes in the lifetime of intracellular singlet oxygen produced in a photosensitized process., *J. Phys. Chem. B*, 2012, **116**, 445–61.
- A. Jiménez-Banzo, M. L. Sagristà, M. Mora and S. Nonell, Kinetics of singlet oxygen photosensitization in human skin fibroblasts., *Free Radic. Biol. Med.*, 2008, **44**, 1926–34.
- V. Vyklický, R. Dēdic, N. Curkaniuk and J. Hála, Spectral- and time-resolved phosphorescence of photosensitizers and singlet oxygen: From in vitro towards in vivo, *J. Lumin.*, 2013, **143**, 729–733.
- L. Chen, L. Lin, Y. Li, H. Lin, Z. Qiu, Y. Gu and B. Li, Effect of oxygen concentration on singlet oxygen luminescence detection, *J. Lumin.*, 2013, DOI: 10.1016/j.jlumin.2013.10.034, in press.
- R. Dēdic, V. Vyklický, A. Svoboda and J. Hála, Phosphorescence of singlet oxygen and 5,10,15,20-tetrakis(1-methyl-4-pyridinio)porphine: Time and spectral-resolved study, *J. Mol. Struct.*, 2009, **924-926**, 153–156.
- R. W. Redmond and J. N. Gamlin, Invited Review A Compilation of Singlet Oxygen Yields from Biologically Relevant Molecules, *Photochem. Photobiol.*, 1999, **70**, 391–475.
- R. Schmidt, K. Seikel and H.-D. Brauer, Determination of the Phosphorescence Quantum Yield of Singlet Molecular Oxygen in Five Different Solvents, *J. Phys. Chem.*, 1989, **93**, 4507–4511.
- J. C. Mullikin, L. J. van Vliet, H. Netten, F. R. Boddeke, G. van der Feltz and I. T. Young, Methods for CCD Camera Characterization, in: H.C. Titus, A. Waks (eds), *Image Acquisition and Scientific Imaging Systems, Proc. SPIE*, 1994, **2173**, 73–84.
- D. Dussault and P. Hoess, Noise performance comparison of ICCD with CCD and EMCCD cameras, *Proc. SPIE*, 2004, **5563**, 195–204.
- A. Prasilov, *Radiometry in Modern Scientific Experiments*, Springer, 2011.
- J. R. Janesick, *Scientific Charge-coupled Devices*, SPIE Press, 2001.
- E. Skovsen, J. W. Snyder, J. D. C. Lambert and P. R. Ogilby, Lifetime and diffusion of singlet oxygen in a cell., *J. Phys. Chem. B*, 2005, **109**, 8570–3.
- I. Zebger, L. Poulsen, Z. Gao, L. K. Andersen and P. R. Ogilby, Singlet Oxygen Images of Heterogeneous Samples: Examining the Effect of Singlet Oxygen Diffusion across the Interfacial Boundary in Phase-Separated Liquids and Polymers, *Langmuir*, 2003, **19**, 8927–8933.
- A. Rück, T. Köllner, A. Dietrich, W. Strauss and H. Schneckenburger, Fluorescence formation during photodynamic therapy in the nucleus of cells incubated with cationic and anionic water-soluble photosensitizers, *J. Photochem. Photobiol. B Biol.*, 1992, **12**, 403–412.
- I. A. Patito, C. Rothmann and Z. Malik, Nuclear transport of photosensitizers during photosensitization and oxidative stress., *Biol. Cell*, 2001, **93**, 285–91.
- M. Niedre, M. S. Patterson and B. C. Wilson, Direct near-infrared luminescence detection of singlet oxygen generated by photodynamic therapy in cells in vitro and tissues in vivo., *Photochem. Photobiol.*, 2002, **75**, 382–91.
- R. B. Vegh, K. M. Solntsev, M. K. Kuimova, S. Cho, Y. Liang, B. L. W. Loo, L. M. Tolbert and A. S. Bommaris, Reactive oxygen species in photochemistry of the red fluorescent protein "Killer Red"., *Chem. Commun. (Camb)*, 2011, **47**, 4887–9.

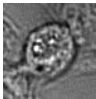
Near-infrared phosphorescence microspectroscopy of single cells

Photochemical & Photobiological Sciences

102



VIS Fluor.



bright
field

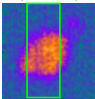
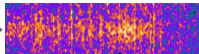
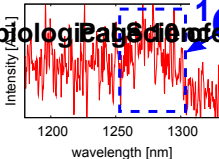


image
>1250nm



spectral image
>1100nm